

Interpretable Cervical Cell Classification: A Comparative Analysis

Nishaanthini Gnanavel
Department of Computer Science
and Engineering
University of Moratuwa
Moratuwa, Sri Lanka
nishaanthini.19@cse.mrt.ac.lk

Prathushan Inparaj
Department of Computer Science
and Engineering
University of Moratuwa
Moratuwa, Sri Lanka
inparaj.19@cse.mrt.ac.lk

Niruthikka Sritharan*
Department of Computer Science
and Engineering
University of Moratuwa
Moratuwa, Sri Lanka
niruthikka.19@cse.mrt.ac.lk

Dulani Meedeniya
Department of Computer Science
and Engineering
University of Moratuwa
Moratuwa, Sri Lanka
dulanim@cse.mrt.ac.lk

Pratheepan Yogarajah
School of Computing, Engineering
and Intelligent Systems
Ulster University
Londonderry, United Kingdom
p.yogarajah@ulster.ac.uk

Abstract—Cervical cancer is a significant global health issue, and traditional screening methods like Pap smears are labor-intensive and may miss some cases. Automation is needed, but it faces challenges in terms of interpretability and data availability. To address this, the paper proposes using Explainable Artificial Intelligence (XAI) techniques like GradCAM, GradCAM++, and LRP to improve the transparency and interpretability of a cervical cell classification model, making it a novel contribution to enhancing the trustworthiness of automated cervical cancer detection. Using the Herlev Dataset, we employ data pre-processing, data augmentation techniques and develop a binary classification model, achieving a 91.94% accuracy with VGG16. The qualitative analysis of XAI methods confirmed that the model relied on nucleus and cytoplasm features, key indicators of malignancy. The least mean image entropy of 2.4849 and steep prediction confidence drop with perturbations quantitatively proved Layer-wise Relevance Propagation (LRP) to be the most effective XAI technique for cervical cell classification.

Keywords—Explainable Artificial Intelligence, Medical image classification, Image entropy, pixel flipping

I. INTRODUCTION

Cervical cancer is the fourth most common cancer among women [1]. Fortunately, it can be treated easily when detected early. Traditionally, the Pap Smear Test and Liquid-Based Cytology Test have been used to detect cancerous and precancerous cells. For instance, features of Pap smear images, such as the nucleus area and the nucleus-to-cytoplasm ratio, can be used to identify abnormal cells. In cancerous cells, the nucleus tends to have a larger area, resulting in a reduced cytoplasm area and a higher ratio. However, conducting these assessments manually is a time-consuming and labour-intensive process

[2]. Moreover, there is a substantial risk of missing one case for every 10 to 15 positive cases. Consequently, there is a pressing need to automate the screening process to enhance efficiency and ensure more accurate results. Numerous classification techniques exist for identifying cancerous cells. However, their deployment is often hindered by concerns related to the interpretability of the decisions they make.

Explainable Artificial Intelligence (XAI) techniques are becoming increasingly popular in the medical field due to their ability to provide transparency and interpretability in decision-making [3]–[5]. Furthermore, when results are explainable and easily understandable, users are more likely to trust the algorithm's decisions, which promotes acceptance of the outcomes. Additionally, these explainable methods aid in identifying and rectifying errors, enabling users to identify potential issues in traditional methods and make manual adjustments, thereby enhancing overall accuracy [6]. To the best of our knowledge, XAI techniques, such as Gradient-weighted Class Activation Mapping (GradCAM) [7], GradCAM++ [8], and Layer-wise Relevance Propagation (LRP) [9], have not been applied for a cervical cell classification in previous research. Therefore, the novel contributions of this study can be stated as follows.

- Utilize XAI techniques in cervical cell classification.
- Provide a comprehensive qualitative analysis of the applied XAI techniques.
- Employ quantitative metrics on XAI techniques applied to the cervical cell classification task.

Accordingly, our main focus lies on the interpretability of the classification models and measuring the explainability using qualitative and quantitative approaches, rather than the cervical cell classification itself. This will help to show the

trustworthiness of the classification model and increase the confidence in using such automated computer-based support tools that interface the medical domain.

II. PREVIOUS WORK

A. Classification

Deep learning (DL) models are widely used in medical image classification [10]–[12]. Certain studies have used traditional methods for the classification of cervical cells. For instance, Bandyopadhyay et al. [13] extracted shape features like area, perimeter, eccentricity, circularity and compactness from the nucleus contours obtained from the segmentation. These features were classified as cancerous and healthy cells, utilizing Random Forest classifier. Several studies have employed DL techniques and used variations of Convolutional Neural Networks (CNNs). Among them, Alsalatie et al. [14] built an ensemble of CNNs from scratch with the 1st stage to classify images between the “normal” and “abnormal” classes and the 2nd stage to classify the abnormal cell images among the 3 malignant classes. VGG-like Net, a more compact version of the VGG network, was employed for faster training and lower computing costs in the classification stage by Allehaibi et al. [15].

Some studies have used pre-trained CNN architectures through Transfer Learning (TL). Accordingly, Tripathi et al. [16] used FASTAI library to implement finetuned ResNet50, ResNet152, VGG16 and VGG19 architectures with cyclic learning rate for binary classification. However, some other studies have further explored the combination of these individual pre-trained models using an ensemble architecture and fusion features. For example, Diniz et al. [17] trained 10 CNNs including EfficientNet models to make predictions for each class and created an ensemble of the 3 best architectures for each class. In addition, Rahaman et al. [18] applied Hybrid Deep Feature Fusion to integrate normalized feature vectors extracted from the 4 DL models. They utilized late fusion for majority voting of pre-trained and fine-tuned VGG16, VGG19, XceptionNet and ResNet50. Moreover, Alquran et al. [19] fused features between the DL descriptors from various structures utilizing principle component analysis (PAC) and Canonical correlation analysis.

In another point of view, several other studies have used the pretrained models for feature extraction. Accordingly, Alquran et al. [20] employed ResNet101 feature extraction and applied five cascading support-vector machine models for classification. Similarly, Chowdary et al. [21] extracted three sets of 4096-dimensional deep features from the second last dense layers of the pre-trained and finetuned VGG19, VGG-F and CaffeNet models. They further extended research directions and generated two hand-crafted descriptors from the image using bag-of-features and linear-binary-patterns. After using PCA on a group-by-group basis to select the most

discriminative features, the chosen features were classified using a multi-layer perceptron model.

B. Explainable Artificial Intelligence

There are several advanced Artificial Intelligence (AI) techniques that are being proposed in the medical domain [3]–[5]. However, even if such approaches perform with high accuracy, the black box nature of such complex models raises skepticism among clinicians, thus emerging as a key barrier to automating medical decisions with these approaches [22], [23]. Therefore, XAI methods are gaining traction in healthcare as an attempt to address the above problem. XAI helps with debugging, identifying bias, and evaluating the reliability of model predictions for critical healthcare decisions. There are a multitude of XAI techniques with certain differences in the parameters like reliability, causality and usability.

Accordingly, GradXcepUNet proposed by Kaur et al. [22] was composed of an Xception model to which original 2D Computerized Tomography (CT) scan images and ground truth segmentation masks labeled as original and liver_only respectively were given as input. Then, the XAI technique, GradCAM, highlighted the critical regions of liver_only class images based on this classification model’s decision. However, they overlooked the assessment of faithfulness, accuracy, stability, interpretability, and fairness of these explanations generated by the chosen XAI technique.

Correspondingly, after attempting to explain the high detection accuracy of the proposed customized CNN model for automated lung disease classification of chest X-ray images with LRP, Pitroda et al. [23] quantitatively compared the explainability of LRP with other XAI methods like Local Interpretable Model Agnostic Explanation (LIME), Deep Taylor Decomposition (DTD), and Guided Backpropagation (GB), using image entropy and pixel flipping performance metric.

Another interesting study by Bhandari et al. [24] utilized Shapley additive explanation (SHAP) and LIME in identifying abnormalities in the kidney. They applied these XAI techniques on a lightweight CNN model that classifies stones, cysts and tumours using CT images.

III. SYSTEM MODEL

A. Process View

The main focus of this study is to evaluate the XAI techniques on cervical cell classification. The input images are extracted from Herlev Dataset [25]. After applying data pre-processing and data augmentation techniques, we develop a supervised binary classification model. In this process, we explore various DL architectures, including VGGnet [26], XceptionNet [27] and EfficientNet [28], to categorise cervical cells as “normal” (healthy) or “abnormal”. Model performance was evaluated using metrics like accuracy, precision, recall, and F1 score on validation and test datasets. After obtaining

the best classifier, several XAI techniques such as GradCAM, GradCAM++ and LRP are applied to highlight the pixels contributing to the classification decision. Then we qualitatively and quantitatively evaluate the performance of the above XAI methods. For quantitative analysis, we used two evaluation metrics namely, image entropy and pixel flipping performance metric [23]. Fig. 1 shows an overview of our proposed methodology.

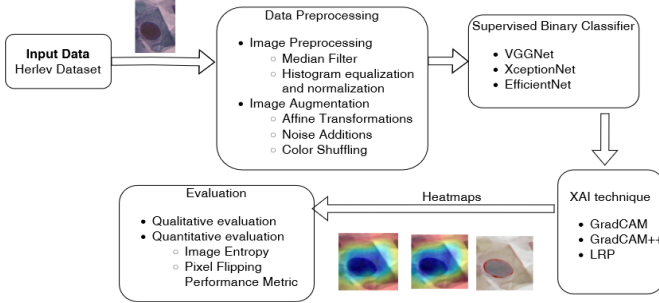


Fig. 1. Overview of the proposed methodology

B. Dataset Description

This study utilizes the cervical cell images from the Herlev dataset. It consists of seven distinct classes. However, considering the scope of this study, we reclassified the dataset into 2 classes: “normal” (images without cancer cells) and “abnormal” (images with cancer cells). Our dataset consists of 917 cell images, with 242 images belonging to the “normal” class and 675 images belonging to the “abnormal” class.

C. Data Preprocessing

Initially, all the images were resized to the same size of 224 x 224 pixels. Then, noise reduction and image enhancements were applied to the images, because the Pap smear images were noisy and had low contrast. We used a median filter for noise reduction, and histogram equalization and normalization to enhance the contrast. The increased contrast assisted the extraction of important information from the image [19].

We applied a random split ratio of 60:20:20 for the original dataset to obtain the corresponding training, validation and test sets. Then, different data augmentations were employed to increase and balance the number of images in each class of the training set [29]. We selected several augmentation techniques among rotation, scaling, translation, shearing, flips, colour channel shuffling, modification of brightness and contrast, addition of Gaussian blur, Gaussian noise, optical distortions, elastic transformations and colour jitter to increase data diversity. Table I provides a summary of the image counts for each class in the training, validation, and test datasets.

D. Classification Model

In this study, we utilized pre-trained models such as VGGNet, XceptionNet, and EfficientNet, which had their weights

TABLE I. DISTRIBUTION OF IMAGES

Class	Original count	After Augmentation		
		Training	Validation	Test
Normal	242	3600	49	49
Abnormal	675	3618	136	136

pre-trained on the ImageNet dataset. To capture more general and generic features, we froze the earlier layers of each CNN model. Then, we made modifications to the latter layers of the network as needed, fine-tuning them by training on the cervical cell dataset to capture more dataset-specific features.

E. Explainable Artificial Intelligence

LRP, GradCAM and GradCAM++ were chosen for explainability over other XAI techniques due to their computational efficiency, theoretical reliability, and adaptability to complex models. LRP can generate explanations in a single forward/backward pass, making it suitable for the experimented intricate CNN classification models. Its computational efficiency, theoretical grounding, and widespread popularity contribute to its trustworthiness. GradCAM and GradCAM++ can be easily integrated with various Artificial Neural Network methods with post hoc flexibility. Even if the model was modified, it could be processed using the same procedure.

Gradient-weighted Class Activation Mapping: GradCAM process begins with a forward pass, where the input image is propagated through the CNN model, and activations are computed across various layers. Subsequently, gradients are computed by backpropagating the predicted score for the target class with respect to the final convolutional layer’s activations. These gradients serve as importance weights for each activation map in that layer, emphasizing the significance of features for the target class based on their gradients. By weighting the activation maps and summing them, a heatmap is generated, representing the regions in the input image that hold the most relevance for the prediction of the target class. Applying Rectified Linear Unit (ReLU) and normalization ensures that the heatmap is appropriately scaled and highlights important areas which helps in understanding the model’s decision-making process.

Gradient-weighted Class Activation Mapping ++: GradCAM++ is an extension of GradCAM, where it improves the visualization accuracy by considering both first and second-order gradients. Initially, a forward pass is performed using the CNN model and the predicted score for the target class is computed. Then the first and second derivatives of the predicted score are calculated considering the activations of the final convolutional layer. The first derivative is used to weigh the importance of activation maps, while the second derivative enhances this weighting. Weights and alphas are calculated to blend and refine the activation maps based on gradients. Then the heatmap is generated by multiplying the normalized weights with the activation maps and aggregation.

Layer-wise Relevance Propagation: LRP goes in reverse over the layers of the network and calculates relevance scores for each neuron in each layer using the weights and activations of the network. Thus, when the output is propagated to the input layer, relevance scores of individual pixels in the image are obtained. This propagation of the prediction backward in the neural model can be achieved using a set of purposely designed propagation rules. This propagation process is subjected to a conservation property, where the relevance score of a neuron is redistributed to the lower layer in equal size [9].

In our experiment, the LRP explanations are obtained for any image with respect to the “abnormal” class. Accordingly, the activation of the output layer (having 2 neurons) is multiplied by a mask to retain the predicted evidence of “abnormal” class only. Following that, while propagating the relevance, dense layers were converted to convolutional layers and max pooling layers were treated as average pooling layers. Further, different rules were applied to different layers, as stated in Table II. Stride and padding are both (1,1) for all the original and newly formed convolutional layers.

TABLE II. LRP IMPLEMENTATION DETAILS FOR VGG16

	Original VGG Layer	Modified Layer	LRP Rule
1	Conv2d (3, 64) Conv2d (64, 64) MaxPool2d	AvgPool2d (2)	z^B γ
2	Conv2d (64, 128) Conv2d (128, 128) MaxPool2d	AvgPool2d (2)	γ γ γ
3	Conv2d (128, 256) Conv2d (256, 256) Conv2d (256, 256) MaxPool2d	AvgPool2d (2)	γ γ γ γ
4	Conv2d (256, 512) Conv2d (512, 512) Conv2d (512, 512) MaxPool2d	AvgPool2d (2)	ϵ ϵ ϵ ϵ
5	Conv2d (512, 512) Conv2d (512, 512) Conv2d (512, 512) MaxPool2d	AvgPool2d (2)	ϵ ϵ ϵ ϵ
6	Linear(25088x4096) Linear(4096x4096) Linear(4096x2)	Conv2d(512, 4096, kernel=(7, 7)) Conv2d(4096, 4096, kernel=(1, 1)) Conv2d(4096, 2, kernel=(1, 1))	0 0 0

F. Evaluation Metrics

Image entropy: measures the disorder or randomness within the pixel values of an image. A higher entropy indicates that the explanation is overly complex, capturing both relevant and irrelevant features in the image. But lower entropy value suggests that the explanation is more focused and less random, potentially highlighting only the significant and relevant regions of the image. Therefore, lower entropy value is desirable as it indicates that the XAI method emphasizes the key features in the image that contribute to the model’s decision.

Pixel flipping performance metric: is based on pixel-flipping approach [30], which involves systematically flipping individual pixels in an image, starting from the most relevant according to the explanation and proceeding to the least relevant. This approach simulates the impact of perturbations

TABLE III. HYPERPARAMETER DETAILS AND PERFORMANCE METRICS

Baseline	Hyperparameters			Performance Metrics			
	Batchsize	Learning Rate	Epochs	Accuracy	Precision	Recall	F1 Score
VGGNet	8	0.001	10	0.92	0.93	0.92	0.91
XceptionNet	16	0.001	10	0.86	0.88	0.86	0.84
EfficientNet	16	0.001	10	0.88	0.90	0.88	0.87

on the image by measuring how the prediction score decreases as pixels are progressively flipped and observes the impact on the explanation generated by the XAI method. Each flipped pixel’s effect on the explanation helps to assess the explanation’s reliability and sensitivity to pixel-level changes. Higher stability, where small pixel alterations result in consistent explanations, indicates a more reliable and robust XAI method.

IV. RESULTS AND DISCUSSION

A. Performance of Classification Model

The obtained performance metrics with the corresponding hyperparameters are shown in Table III. It can be observed that VGG16 and EfficientNet performed well in cervical cell classification. However, since it was observed that models without skip connections offer a more streamlined architecture for layerwise relevance propagation, the VGG16 based model was chosen as the primary option. The confusion matrix in Fig. 2 further validates that the model classifies most of the cervical cell images correctly.

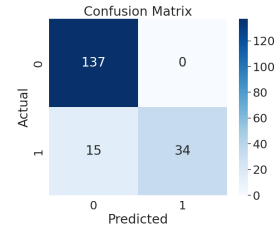


Fig. 2. Confusion Matrix of the customized VGG16 Model

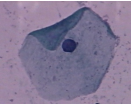
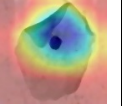
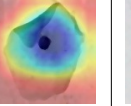
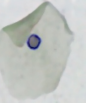
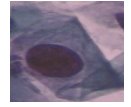
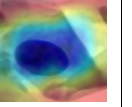
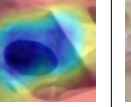
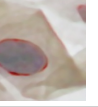
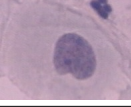
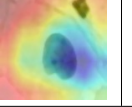
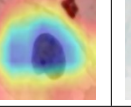
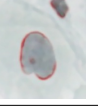
In this VGG16 architecture based model, a global average max pooling layer was incorporated. Further, the neuron count in final layer was modified and the model was configured to use a softmax activation, enabling it to predict class probabilities for the two target classes: “normal” and “abnormal.” This tailored approach aligned well with the study’s objectives.

B. Performance of XAI techniques

• Qualitative analysis

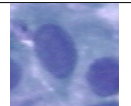
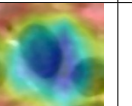
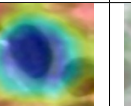
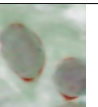
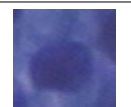
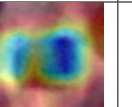
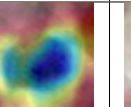

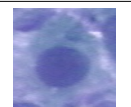
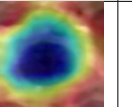
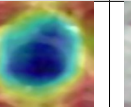
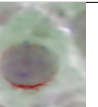
To visually compare the performance of GradCAM, GradCAM++ and LRP, three images that were predicted correctly and incorrectly with highest confidence were chosen. Explanations were generated for each of those by the 3 XAI techniques and overlaid on the original images. These images and overlaid explanations are illustrated in Table IV and Table V.

TABLE IV. EXPLANATIONS FOR BEST PREDICTIONS

No	Original Image	GradCAM	GradCAM++	LRP
image-1				
image-2				
image-3				

Upon visual inspection, the GradCAM and GradCAM++ activation maps in Table IV have highlighted the regions within the nucleus of the cell and its associated cytoplasm, which are the main indicators of malignancy in cervical cells. GradCAM++ activation maps have more regions within the nucleus with higher activations and the highlighted regions are sharper and well defined than in GradCAM activation maps. Considering the LRP explanations, however, the cytoplasm region, which also contributes to the malignancy of a cell, has not been highlighted. It has only outlined the nuclei clearly in all three images as evidence for the predicted class. The small nucleus of image-1 has a negative effect on the “abnormal” class with respect to which the LRP explanations were generated. Consequently, that nucleus has been outlined in blue. In contrast, the large nuclei of cells in image-2 and image-3 that belong to “abnormal” class have been outlined appropriately in red due to their positive contribution towards model’s decision. Thus, these three explanations confirm that the classifier’s decisions are correctly based on the nuclei and/or cytoplasm, and not other spurious features.

TABLE V. EXPLANATIONS FOR WORST PREDICTIONS

No	Original Image	GradCAM	GradCAM++	LRP
image-4				
image-5				
image-6				

Most malignant cells have larger nucleus size compared to benign cells. Yet, the “normal” images in Table V, are observed to have nuclei in size similar to that of abnormal cells. Deceived by this large nuclei, which is highlighted by the higher activations in GradCAM and GradCAM++ explanations, and is outlined in red by the LRP explanations,

the model has incorrectly classified these cells as “abnormal”.

• Quantitative analysis

The average image entropy of all the images in the test set were obtained for each of the 3 XAI techniques. Table VI indicates these entropy values. GradCAM++ yields a significantly higher mean image entropy indicating a detailed explanation, but it shows that it exhibits greater complexity compared to the other two XAI methods and it contains more than relevant information in its explanation. GradCAM with the mean image entropy slightly higher than that of LRP suggests that it highlights important regions of the input images, but there is still some variability in the highlighted region. LRP with its least mean image entropy value suggests that it has highlighted only the regions that significantly contribute to the underlying classifier’s decision, potentially making it a suitable choice when simplicity and clarity are paramount.

TABLE VI. MEAN IMAGE ENTROPY FOR XAI TECHNIQUES

XAI Technique	GradCAM	GradCAM++	LRP
Mean Image Entropy	2.6567	5.3688	2.4849

Next, an image that was predicted correctly as “abnormal” with high confidence was chosen. Using each XAI technique, the pixels in the region that contributed most to the model’s decision were flipped in different percentages. Subsequently, the manner in which the prediction confidence relevant to the “abnormal” class changed is demonstrated in Fig. 3.

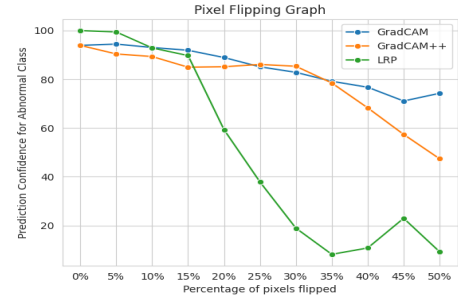


Fig. 3. Pixel Flipping Graph

It is evident from Fig. 3 that the prediction class has changed to “normal” when more than 25% of pixels considered important by LRP are flipped. This steep drop in LRP curve compared to other curves indicates that LRP has identified the region most important to model’s decision, since significant perturbations in that region result in drastic changes in model’s decision and prediction confidence. However, for smaller perturbations with a lower number of pixels being flipped, the prediction confidence has not changed considerably and this indicates the robustness of LRP.

Since the proposed solution introduced a novel dimension by applying XAI techniques, including GradCAM, GradCAM++, and LRP for the first time to the domain of cervical cell classification and provided a comprehensive qualitative

and quantitative analysis of XAI techniques for the cervical cell classification task, we cannot be directly compared with existing State-of-the-Art (SOTA) studies, due to the absence of prior studies utilizing these techniques in this specific domain.

As future extensions, more quantitative metrics that explore the faithfulness, stability, fairness and interpretability of XAI techniques could be applied for generated explanations and such explanations can be validated by a medical practitioner, facilitating the fault detections and improved trustworthiness of AI techniques in health settings.

V. CONCLUSION

This study presented an approach to classify cervical cell images as “normal” or “abnormal” using different CNN architectures. The VGG16 based model exhibited a high accuracy of 91.94%. XAI techniques such as GradCAM, GradCAM++ and LRP were applied to explore the interpretability of this classifier. The qualitative comparison of these explanations showed that the model did base its decisions appropriately on nuclei and cytoplasm of the cell, which are the true indicators of malignancy. While GradCAM and GradCAM++ explanations highlighted both nucleus and cytoplasm regions, LRP explanations outlined the nucleus alone. However, with the least mean image entropy and steepest prediction confidence drop for significant perturbations, LRP proves to be explanation technique with lower complexity identifying only the most relevant region to the underlying classifier’s decision.

REFERENCES

- [1] Y. Fan, Z. Tao, J. Lin, and H. Chen, “An encoder-decoder network for automatic clinical target volume target segmentation of cervical cancer in ct images,” *International Journal of Crowd Science*, vol. 6, no. 3, pp. 111–116, 2022.
- [2] C. Seibold, J. Künzel, A. Hilsmann, and P. Eisert, “From explanations to segmentation: using explainable ai for image segmentation,” *arXiv preprint arXiv:2202.00315*, 2022.
- [3] S. Dasanayaka, V. Shantha, S. Silva, T. Ambegoda, and D. Meedeniya, “Interpretable machine learning for brain tumor analysis using MRI,” in *Proceedings of the 2nd International Conference on Advanced Research in Computing (ICARC)*, Belihuloya, Sri Lanka, 2022, pp. 212–217.
- [4] S. Dasanayaka, V. Shantha, S. Silva, D. Meedeniya, and T. Ambegoda, “Interpretable machine learning for brain tumour analysis using mri and whole slide images,” *Software Impacts*, vol. 13, p. 100340, 2022.
- [5] L. Gamage, U. Isuranga, S. De Silva, and D. Meedeniya, “Melanoma skin cancer classification with explainability,” in *Proceedings of the 3rd International Conference on Advanced Research in Computing (ICARC)*, Belihuloya, Sri Lanka: IEEE, 2023, pp. 30–35.
- [6] S. Wickramanayake, S. Rasnayaka, M. Gamage, D. Meedeniya, and I. Perera, “Explainable artificial intelligence for enhanced living environments: A study on user perspective,” ser. *Advances in Computers*. Elsevier, 2023.
- [7] R. R. Selvaraju, M. Cogswell, A. Das, R. Vedantam, D. Parikh, and D. Batra, “Grad-cam: Visual explanations from deep networks via gradient-based localization,” in *Proceedings of the IEEE international conference on computer vision*, 2017, pp. 618–626.
- [8] A. Chattopadhyay, A. Sarkar, P. Howlader, and V. N. Balasubramanian, “Grad-cam++: Generalized gradient-based visual explanations for deep convolutional networks,” in *IEEE winter conference on applications of computer vision (WACV)*. IEEE, 2018, pp. 839–847.
- [9] S. Bach, A. Binder, G. Montavon, F. Klauschen, K.-R. Müller, and W. Samek, “On pixel-wise explanations for non-linear classifier decisions by layer-wise relevance propagation,” *PLoS one*, vol. 10, no. 7, p. e0130140, 2015.
- [10] N. Wijethilake, D. Meedeniya, C. Chitraranjan, I. Perera, M. Islam, and H. Ren, “Glioma survival analysis empowered with data engineering—a survey,” *IEEE Access*, vol. 9, pp. 43 168–43 191, 2021.
- [11] D. Meedeniya, H. Kumarasinghe, S. Kolonne, C. Fernando, I. De la Torre Díez, and G. Marques, “Chest x-ray analysis empowered with deep learning: A systematic review,” *Applied Soft Computing*, vol. 126, p. 109319, 2022.
- [12] D. Meedeniya and I. Rubasinghe, “A review of supportive computational approaches for neurological disorder identification,” in *Interdisciplinary Approaches to Altering Neurodevelopmental Disorder*, T. Wadhera and D. Kakkar, Eds. IGI Global, 2020, ch. 16, pp. 271–302.
- [13] H. Bandyopadhyay and M. Nasipuri, “Segmentation of pap smear images for cervical cancer detection,” in *IEEE Calcutta Conference (CALCON)*. Kolkata, India: IEEE, 2020, pp. 30–33.
- [14] M. Alsallat, H. Alquran, W. A. Mustafa, Y. Mohd Jacob, and A. Ali Alayed, “Analysis of cytology pap smear images based on ensemble deep learning approach,” *Diagnostics*, vol. 12, no. 11, p. 2756, 2022.
- [15] K. H. S. Allehaibi, L. E. Nugroho, L. Lazuardi, A. S. Prabuono, T. Mantoro *et al.*, “Segmentation and classification of cervical cells using deep learning,” *IEEE Access*, vol. 7, pp. 116 925–116 941, 2019.
- [16] A. Tripathi, A. Arora, and A. Bhan, “Classification of cervical cancer using deep learning algorithm,” in *5th International Conference on Intelligent Computing and Control Systems (ICICCS)*. Madurai, India: IEEE, 2021, pp. 1210–1218.
- [17] D. N. Diniz, M. T. Rezende, A. GC Bianchi, C. M. Carneiro, E. JS Luz, G. JP Moreira, D. M. Ushizima, F. NS de Medeiros, and M. JF Souza, “A deep learning ensemble method to assist cytopathologists in pap test image classification,” *Journal of Imaging*, vol. 7, no. 7, p. 111, 2021.
- [18] M. M. Rahaman, C. Li, Y. Yao, F. Kulwa, X. Wu, X. Li, and Q. Wang, “Deepcervix: A deep learning-based framework for the classification of cervical cells using hybrid deep feature fusion techniques,” *Computers in Biology and Medicine*, vol. 136, p. 104649, 2021.
- [19] H. Alquran, M. Alsallat, W. A. Mustafa, R. A. Abdi, and A. R. Ismail, “Cervical net: A novel cervical cancer classification using feature fusion,” *Bioengineering*, vol. 9, no. 10, p. 578, 2022.
- [20] H. Alquran, W. A. Mustafa, I. A. Qasmieh, Y. M. Yacob, M. Alsallat, Y. Al-Issa, and A. M. Alqudah, “Cervical cancer classification using combined machine learning and deep learning approach,” *Comput. Mater. Contin.*, vol. 72, no. 3, pp. 5117–5134, 2022.
- [21] G. J. Chowdary and P. Yogarajah, “Nucleus segmentation and classification using residual se-unet and feature concatenation approach incervical cytopathology cell images,” *Technology in Cancer Research & Treatment*, vol. 22, p. 15330338221134833, 2023.
- [22] A. Kaur, G. Dong, and A. Basu, “Gradxcepunet: Explainable ai based medical image segmentation,” in *International Conference on Smart Multimedia*. Marseille, France: Springer, 2022, pp. 174–188.
- [23] V. Pitroda, M. M. Fouda, and Z. M. Fadlullah, “An explainable ai model for interpretable lung disease classification,” in *IEEE International Conference on Internet of Things and Intelligence Systems (IoTIS)*. Bandung, Indonesia: IEEE, 2021, pp. 98–103.
- [24] M. Bhandari, P. Yogarajah, M. S. Kavitha, and J. Condell, “Exploring the capabilities of a lightweight cnn model in accurately identifying renal abnormalities: Cysts, stones, and tumors, using lime and shap,” *Applied Sciences*, vol. 13, no. 5, p. 3125, 2023.
- [25] J. Jantzen, J. Norup, G. Dounias, and B. Bjerregaard, “Pap-smear benchmark data for pattern classification,” *Nature inspired smart information systems (NiSIS 2005)*, pp. 1–9, 2005.
- [26] K. Simonyan and A. Zisserman, “Very deep convolutional networks for large-scale image recognition,” *arXiv preprint arXiv:1409.1556*, 2014.
- [27] F. Chollet, “Xception: Deep learning with depthwise separable convolutions,” in *Proceedings of the IEEE conference on computer vision and pattern recognition*, 2017, pp. 1251–1258.
- [28] M. Tan and Q. Le, “Efficientnet: Rethinking model scaling for convolutional neural networks,” in *International conference on machine learning*. PMLR, 2019, pp. 6105–6114.
- [29] D. Meedeniya, *Deep Learning: A Beginners’ Guide*. CRC Press LLC, 2023. [Online]. Available: www.routledge.com/9781032473246
- [30] J. Kauffmann, K.-R. Müller, and G. Montavon, “Towards explaining anomalies: a deep taylor decomposition of one-class models,” *Pattern Recognition*, vol. 101, p. 107198, 2020.